electronics

MDPI

Article

A Broadband Mode Converter Antenna for Terahertz Communications

Biswash Paudel *, Xue Jun Li * and Boon-Chong Seet

Department of Electrical and Electronic Engineering, Auckland University of Technology, Auckland 1010, New Zealand; boon-chong.seet@aut.ac.nz

* Correspondence: biswash.paudel@autuni.ac.nz (B.P.); xuejun.li@aut.ac.nz (X.J.L.)

Abstract: The rise of artificial intelligence (AI) necessitates ultra-fast computing, with on-chip terahertz (THz) communication emerging as a key enabler. It offers high bandwidth, low power consumption, dense interconnects, support for multi-core architectures, and 3D circuit integration. However, transitioning between different waveguides remains a major challenge in THz systems. In this paper, we propose a THz band mode converter that converts from a rectangular waveguide (RWG) (WR-0.43) in TE_{10} mode to a substrate-integrated waveguide (SIW) in TE_{20} mode. The converter comprises a tapered waveguide, a widened waveguide, a zigzag antenna, and an aperture coupling slot. The zigzag antenna effectively captures the electromagnetic (EM) energy from the RWG, which is then coupled to the aperture slot. This coupling generates a quasi-slotline mode for the electric field (E-field) along the longitudinal side of the aperture, exhibiting odd symmetry akin to the SIW's TE_{20} mode. Consequently, the TE_{20} mode is excited in the symmetrical plane of the SIW and propagates transversely. Our work details the mode transition principle through simulations of the EM field distribution and model optimization. A back-to-back RWG TE_{10}-to-TE_{10} mode converter is designed, demonstrating an insertion loss of approximately 5 dB over the wide frequency range band of 2.15–2.36 THz, showing a return loss of 10 dB. An on-chip antenna is proposed which is fed by a single higher-order mode of the SIW, achieving a maximum gain of 4.49 dB. Furthermore, a balun based on the proposed converter is designed, confirming the presence of the TE_{20} mode in the SIW. The proposed mode converter demonstrates its feasibility for integration into a THz-band high-speed circuit due to its efficient mode conversion and compact planar design.

Keywords: zigzag antenna; rectangular waveguide; substrate integrated waveguide; aperture coupling slot; balun

Academic Editors: Giovanni Andrea Casula and Dimitra I. Kaklamani

Received: 12 December 2024
Revised: 16 January 2025
Accepted: 25 January 2025
Published: 29 January 2025

Citation: Paudel , B.; Li, X.J.; Seet, B.-C. A Broadband Mode Converter Antenna for Terahertz Communications. *Electronics* **2025**, *14*, 551. https://doi.org/10.3390/electronics14030551

1. Introduction

The ever-increasing number of mobile subscribers and their demand for broadband and high-speed wireless communication drive operating frequencies into the terahertz (THz) band. Compared with the microwave band, the THz band offers a larger channel bandwidth and thus a higher data rate, which is expected to exceed 10 Gbps, making them suitable for various applications such as intra- and inter-chip communication, augmented reality (AR), virtual reality (VR), biomedical imaging, and THz spectroscopy [1–3].

Despite these advantages, research on THz communication is still in its infancy due to the challenges of integrating THz communication components with other RF components. Rectangular waveguides (RWGs) are popular for THz transmission lines and components because of their high-quality factor, low insertion loss, and mechanical robustness. However, their bulky nature makes direct integration with the planar THz circuit difficult [4].

Substrate-integrated waveguides (SIWs) facilitate planar integration of THz circuits, offering compatibility with other RF components. The SIW is a planar structure comprising a dielectric substrate with metallic vias along either side enclosed by top and bottom metallic layers. This enclosed configuration and the gap between the vias effectively suppress electromagnetic (EM) wave leakage and interference, making the SIW ideal for high-density integration of THz circuits. Additionally, the SIW can be mass-produced using printed circuit board (PCB) technologies, offering enhanced performance stability due to reduced fabrication tolerances [5,6].

Advanced on-chip communications are needed to support the ultra-high-speed computing tasks required by the recent boom in AI. On-chip THz communication is a promising option for contemporary computing systems, supporting these technologies for future AI development. High-density interconnects, multi-core or many-core computing architectures [1,7], on-chip THz communications [8], and three-dimensional (3D) circuit integration can all be made possible by on-chip THz communications. Mode converter antennas are therefore necessary for THz systems, which frequently call for switching between various waveguide types. However, current research on converters primarily focuses on frequencies from microwave to millimeter waves [9–12]. The lack of an efficient mode converter antenna design remains a bottleneck for high-speed THz communication systems. With advancements in SIW technology, there is a growing interest in exploring higher-order modes for applications such as antennas [13,14], antenna arrays [15], and power combiners and dividers [16]. However, when the SIW operates in higher-order modes, the fundamental (dominant) mode is also typically present, making it challenging to isolate or suppress the undesired mode. Various mode converters have been proposed to address this issue.

In this paper, we propose a single higher-order mode converter in the THz band for a standard RWG (WR-0.3) to a SIW, enabling parallel integration with a wider operating frequency bandwidth [4]. Since RWGs and SIWs are structurally dissimilar and oriented along different axes, the transition from an RWG in TE_{10} mode to a SIW in TE_{20} mode employs a tapered waveguide to align the E-field orientation. The design reduces the complexity and cost by changing the converter from a non-planar RWG to a planar SIW, paving the way for complete front-end THz circuits on a single dielectric substrate. This approach facilitates simple fabrication, packaging, and assembly [5]. The resulting structure supports the integration of passive components, such as antennas [13,14], filters [17], and resonators, on a single substrate with low-loss performance. The rest of this paper is organized as follows: Section 2 reviews the associated works; Section 3 discusses the propagating modes in the SIW; Section 4 provides the mode converter design and examines the results; Section 5 proposes an on-chip antenna based on a dielectric resonator fed by the TE_{20} mode of the SIW; Section 6 presents a balun based on the proposed mode converter; and finally, Section 7 concludes the paper.

2. Related Work

The RWG-to-SIW converter is crucial for improving RF circuit integration, offering benefits like circuit miniaturization, compatibility with test equipment, ease of fabrication, and seamless mode conversion between technologies. While SIWs and RWGs have different structures, the SIW retains the RWG's high-Q factor, internal field distribution, and cutoff frequency characteristics, along with its advantages such as a low profile, low cost, and easy integration. These properties enable conversion in both planar [4,12,18] and right-angle designs [19,20].

Several RWG-to-SIW conversions have been reported in the literature. In [4], Cano et al. proposed using an air-filled RWG with a four-section height-stepped waveguide and a single-width-stepped transformer to achieve conversion in the Q-band without a dielectric probe. Similarly, the authors of [12] developed a back-to-back RWG-SIW-RWG

converter for the 23.8–40 GHz range, incorporating a ridged waveguide with a central bulge to concentrate power and directing EM energy through the bulged section into the SIW. Another converter, proposed in [18], employs aperture coupling between the H-plane of the RWG and SIW, using a narrow slot etched into both structures with the SIW placed atop the RWG. A T-junction based on this design operates in the 26.3–30.6 GHz range.

A back-to-back wideband RWG-to-SIW converter interconnected at 220 GHz, operating in the 0.17–0.26 THz range, was proposed in [19]. The RWG is placed perpendicular to the SIW, and the conversion is achieved using a stepped dielectric transformer and coupling aperture without additional components inside the waveguide. Similarly, the authors of [21] proposed a wideband SIW-to-WR-28 (RWG) converter using a bent waveguide structure, integrating a ridged step in the RWG and a septum in the SIW cavity. Another air-filled RWG-to-SIW converter, fabricated using PCB technology and operating in the V-band, was proposed in [20]. This converter employs an antenna design with a cavity-backed aperture to convert the TE_{10} mode from a horizontal to a vertical direction. While being compact, this design requires multiple substrate layers, making it unsuitable for parallel system integration.

Most existing designs convert the fundamental TE_{10} mode of the RWG to the TE_{10} mode of the SIW and operate in the low-frequency band, with limited research focusing on achieving higher-order modes. The approach proposed in [22] employs two-step conversion, specifically by converting a quasi-TEM microstrip line mode to a grounded slot-line and then to the TE_{20} mode SIW. Another method demonstrated in [6] uses a substrate with three metal layers: a microstrip on the first layer, a slot aperture in the second, and an SIW on the second and third layers. A broadband converter by the authors of [9] converts the TE_{10} mode of the RWG to the TE_{20} mode of the SIW using a dipole antenna and slot-line. Finally, the authors of [23] proposed a TE_{10}–TE_{30} mode converter which employs a self-compensating phase-shifting technique and power divider to modulate the guided wave's amplitude and phase, achieving conversion efficiency of over 95%.

Some research has explored higher-order modes but primarily in the microwave-to-millimeter wave frequency range [23,24]. However, operating in higher-order modes, such as TE_{30} or TE_{40}, requires extremely precise control over the dimensions and alignment to achieve proper impedance matching, adding significant design complexity at THz frequencies. Additionally, the cutoff frequencies for higher-order modes beyond TE_{20} are higher, making them more susceptible to propagation losses and reducing efficiency. In practice, challenges such as fabrication imperfections and variations in substrate properties make it difficult to distribute power evenly among the multiple maxima of the E-field [25]. While higher-order modes, such as TE_{40}, have been effectively excited in certain designs, such as antenna arrays [15], this is typically achieved through the combination of two parallel TE_{20} modes, which may not be suitable for all applications in the THz band.

3. Modes of Propagation in SIW

The SIW is a type of planar waveguide technology for high-density millimeter wave and THz circuits and antennas. It modifies the RWG by using metallic via rows on dielectric substrates with top and bottom metal layers. A higher dielectric constant increases the transmission loss but improves EM wave confinement [5,26].

The design of an SIW involves multiple full-wave simulations and an optimization process to achieve optimal results. The initial design equations for the width of a SIW are provided in [27] to expedite the process. Since the propagation modes of an SIW are similar to those of an RWG, the same cutoff frequency equation can be applied to the SIW [28].

The final optimized value for the width of the SIW (w_{siw}) was 95 µm, the diameter of the vias (d_{via}) was 25 µm, the pitch of the vias (p_{via}) was 25 µm, and the substrate thickness (h_{sub}) was 20 µm. The substrate material was polyimide with a dielectric constant (ϵ_r) of 3.5

and a loss tangent (tan δ) of 0.008. Additionally, design guidelines for the diameter-to-pitch ratio can be found in [5].

Figure 1 shows the SIW modes, where the 1.66–2.5 THz range corresponds to the dual-mode region, allowing both TE_{10} and TE_{20} modes to be excited and propagated. Figure 2 depicts the E-field distribution in the dominant TE_{10} and TE_{20} modes. The waveguide theory [29] states that in the case of a SIW in TE_{mn} mode, the electric and magnetic field components are as follows:

$$E_x = \frac{j\omega\mu n\pi}{k_c^2 b} A\cos\frac{m\pi x}{a}\sin\frac{n\pi y}{b}e^{-j\beta z} \tag{1}$$

$$E_y = \frac{-j\omega\mu m\pi}{k_c^2 a} A\sin\frac{m\pi x}{a}\cos\frac{n\pi y}{b}e^{-j\beta z} \tag{2}$$

where a and b are the width and height of the waveguide, respectively. In a TE mode, there is no electric field component in the z-direction because the electric field is transverse to the direction of propagation along the z-axis of the waveguide ($E_z = 0$):

$$H_x = \frac{j\beta m\pi}{k_c^2 a} A\sin\frac{m\pi x}{a}\cos\frac{n\pi y}{b}e^{-j\beta z} \tag{3}$$

$$H_y = \frac{j\beta n\pi}{k_c^2 b} A\cos\frac{m\pi x}{a}\sin\frac{n\pi y}{b}e^{-\beta z} \tag{4}$$

$$H_z = A\cos\frac{m\pi x}{a}\cos\frac{n\pi y}{b}e^{-j\beta z} \tag{5}$$

$$\beta = \sqrt{k^2 - k_c^2}\,,\ k = \omega\sqrt{\mu\epsilon_o\epsilon_r}\,,\ k_c = \sqrt{\left(\frac{m\pi}{a}\right)^2 + \left(\frac{n\pi}{b}\right)^2} \tag{6}$$

In the case of an SIW operating in TE_{20} (m = 2, n = 0) mode and solving Equations (1)–(5), the field components become as follows:

$$E_y = -A_{20}\frac{j\omega\mu w_{\text{siw}}}{2\pi}\sin\left(\frac{2\pi}{w_{\text{siw}}}x\right)e^{-j\beta z} \tag{7}$$

$$H_x = A_{20}\frac{j\beta w_{\text{siw}}}{2\pi}\sin\left(\frac{2\pi}{w_{SIW}}x\right)e^{-j\beta z} \tag{8}$$

$$H_z = A_{20}\cos\left(\frac{2\pi}{w_{\text{siw}}}x\right)e^{-j\beta z} \tag{9}$$

$$E_x = E_z = H_y = 0 \tag{10}$$

where ω, A_{20}, and w_{siw} are the angular frequency, the amplitude constant in TE_{20} mode and the width of the SIW, respectively. Hence, there is no electric field component in the x- and z-directions and no magnetic field component in the y-direction.

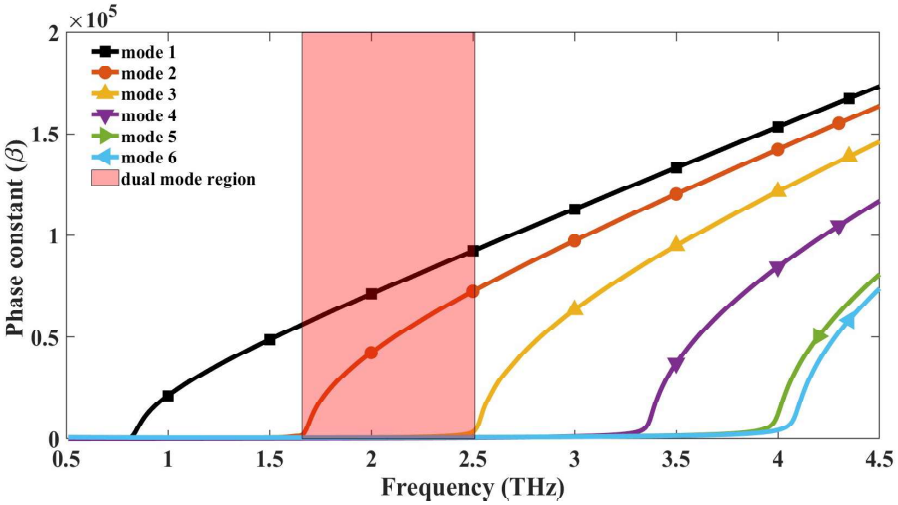

Figure 1. Simulated dispersion curves of SIW.

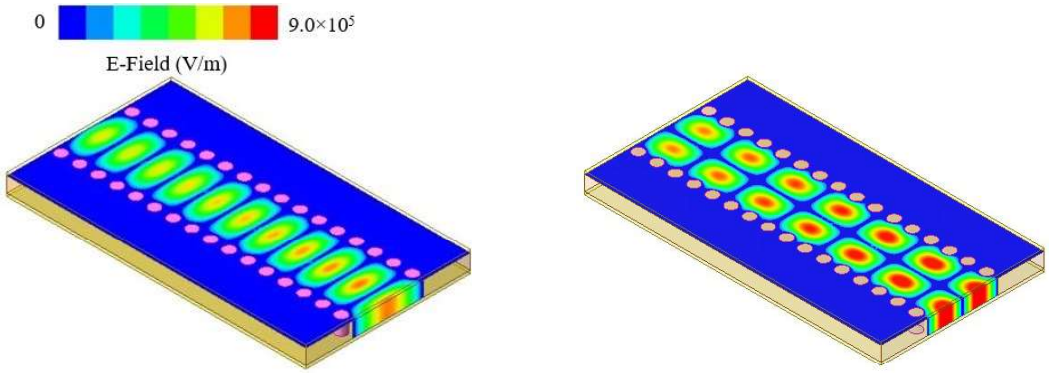

(a) (b)

Figure 2. Electric field distribution at 2.25 THz of (**a**) TE_{10} and (**b**) TE_{20} modes in the SIW.

For Equation (7), if the value of $x = w_{\mathrm{siw}}/2$, then the electric field component in the y direction becomes zero. Hence, the electric field is symmetric about $x = w_{\mathrm{siw}}/2$, exhibiting equal electric field magnitudes on both sides but with the opposite sign for the TE_{20} mode. Thus, a symmetric plane can be regarded as an electric wall or virtual ground [9]. Based on this, it is possible to couple EM energy propagating in the TE_{20} mode of the SIW while suppressing the dominant TE_{10} mode using a suitable excitation method.

4. Investigation of the RWG TE_{10} to SIW TE_{20} Mode Converter

4.1. Designing the Mode Converter

The detailed configuration of the mode converter is shown in Figure 3. It consists of standard RWG WR-0.43, tapered RWG, broadened waveguide, zigzag antenna, aperture coupling slot, and a single polyimide substrate enclosed by the top and bottom metal layers with vias on either side. The center-fed zigzag antenna and coupling slot are incorporated as the top metallic layer, which is extended into the tapered RWG, where the y-polarized electric field in TE_{10} mode is transformed into the TE20 mode with z-polarized electric fields [16].

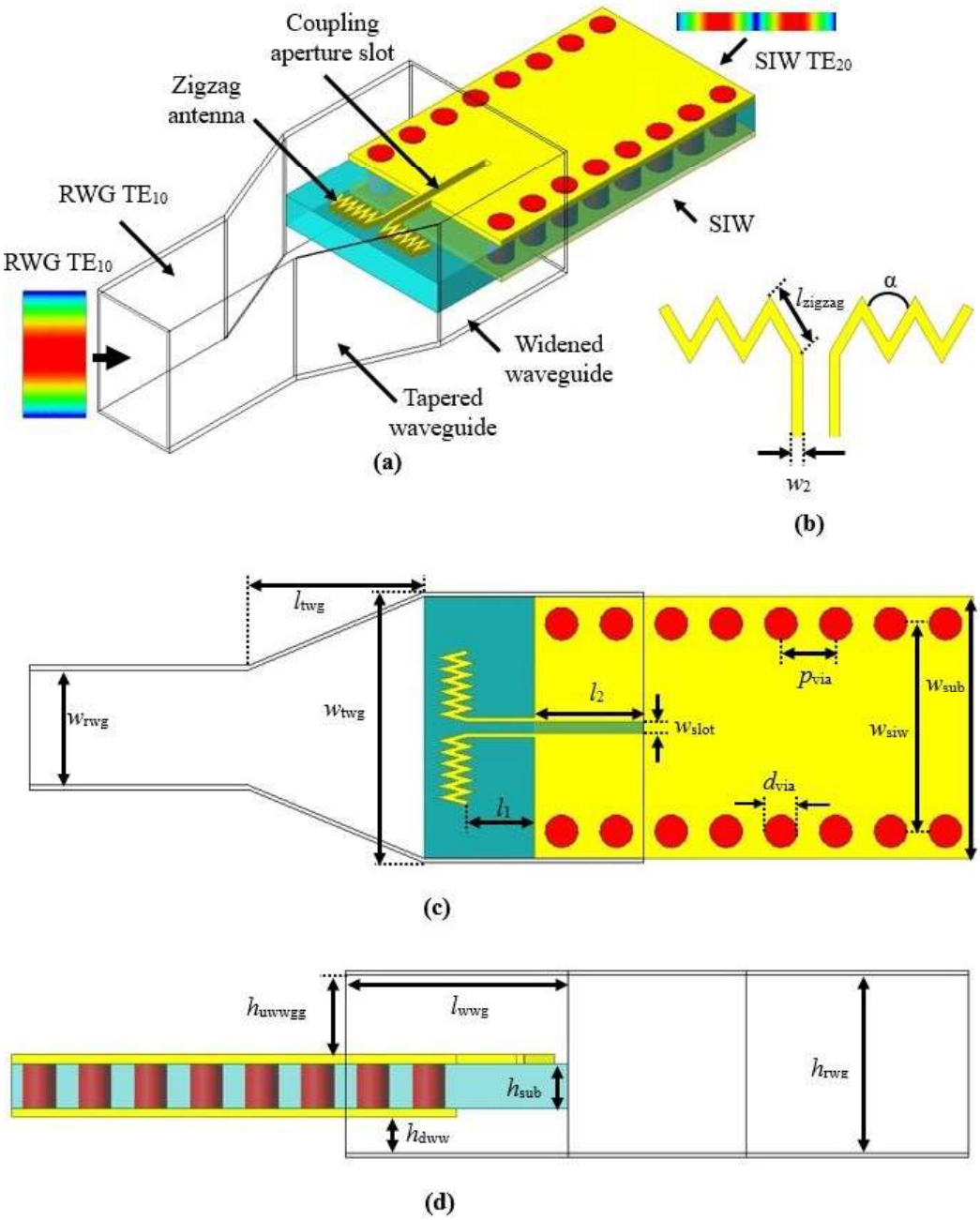

Figure 3. RWG TE_{10} mode to SIW TE_{20} mode converter: (**a**) isometric view, (**b**) zigzag antenna, (**c**) top view, and (**d**) side view.

The first mode conversion occurs at the connection between the extended RWG and the center-fed zigzag antenna. Unlike the dipole antenna, which has two equal arm lengths, the zigzag antenna was selected for its higher degree of design flexibility, allowing adjustment of both arm lengths and the angle between the arms. This flexibility supports the formation of standing waves along its arm, where the current alternates through the angled segments. These alternating currents create multiple radiating elements, resulting in constructive interference which enhances radiation efficiency, energy coupling, and directivity [30]. Furthermore, the zigzag pattern increases the antenna's effective electrical length without increasing its physical size, making it an optimal choice for achieving the desired performance in our mode converter [1,31].

Under perfect impedance-matched conditions, the incoming EM wave couples with the zigzag antenna at this resonance frequency, determined by its arms' length (l_{zigzag}) and

their angle (α). Once the EM energy is coupled into the zigzag antenna, it captures the TE_{10} mode RWG, and the energy is then propagated transversely through the antenna to the aperture coupling slot. The coupling slot supports an E-field mode, also known as the quasi-slotline mode or odd mode, which has equal magnitudes but in opposite directions across the symmetrical plane. This E-field of the odd mode from the slot-line is similar to the E-field of the TE_{20} mode of the SIW, as shown in Figure 4. Both the quasi-slotline mode and the SIW's TE_{20} mode exhibit similar cross-sectional E-field distributions across the symmetrical plane (x-y plane), resembling an electric wall. As a result, EM coupling between the quasi-slotline mode and SIW TE_{20} mode is achieved [9,10,19]. Thus, the zigzag antenna plays a significant role in capturing the incoming energy from the RWG, converting it into the odd mode through the slot-line and facilitating coupling with the SIW in TE_{20} mode, allowing the mode conversion.

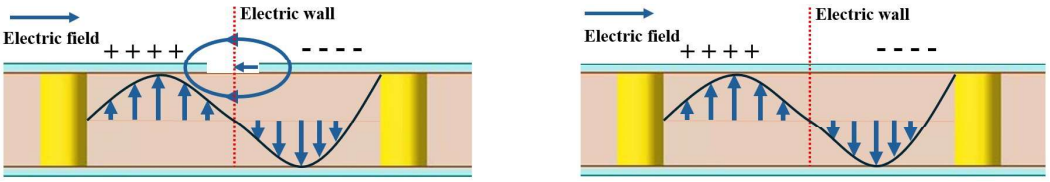

(a) (b)

Figure 4. Electric field distribution for (**a**) quasi-slotline mode and (**b**) TE_{20} SIW mode.

4.2. Simulated E-Field Results

Figure 5 shows the simulated results of the electric field distribution of the proposed mode converter which effectively facilitated the mode conversion from the RWG TE_{10} to SIW TE_{20} over a wide frequency range from 2.16 to 2.35 THz. Although Figure 1 shows the dual-mode region of the SIW as being from 1.6 to 2.5 THz, the proposed mode converter only excites and propagates the SIW's TE_{20} mode, thus isolating the dominant TE_{10} mode of the SIW.

Furthermore, we checked the proposed converter's attenuation capabilities in other SIW modes. Figure 6 shows the electric field distribution of the proposed converter when the SIW was applied with the TE_{10} and TE_{20} modes at a frequency of 2.25 THz. It became clear that the TE_{10} mode from the SIW could not become coupled with the RWG, whereas the TE_{30} mode was not even able to propagate inside the SIW because the operating frequency range of the converter was in the cutoff frequency region for the TE_{30} mode and higher modes.

Based on the simulated results of the electric field distribution, the guided TE_{10} mode of the RWG was converted into a quasi-slotline mode with an odd-mode E-field distribution across the slot, achieved through the resonance of the zigzag antenna. The discontinuity in the tangential electric field prevents the generation of an even-mode electric field over a typical slot line according to Maxwell's boundary equations [32]. As a result, the TE_{20} mode was comparable to the odd-mode electric field pattern of the slot-line. Nevertheless, in some cases, such as the conductor-backed slot-line (CBSL), an even mode can be generated [33]. However, this even-mode corresponds to the TE_{20} mode of the SIW [9], thereby isolating the dominant TE_{10} mode in the dual-mode area of the SIW.

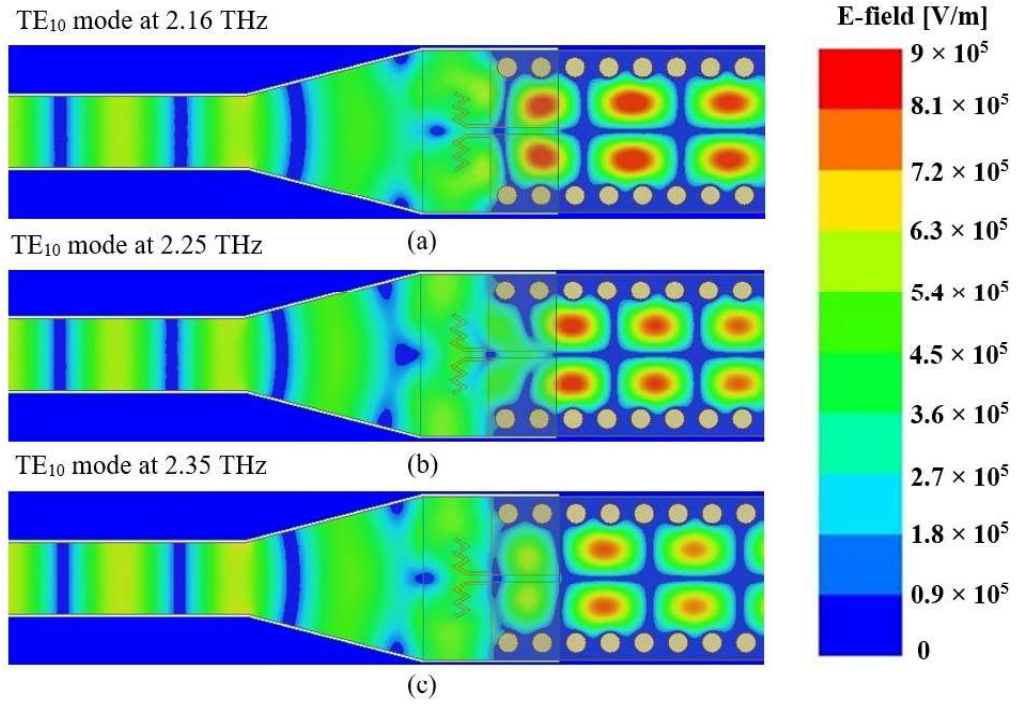

Figure 5. Simulated E-field distribution of the proposed RWG TE_{10} mode to SIW TE_{20} mode converter at (**a**) 2.16, (**b**) 2.25, and (**c**) 2.35 THz.

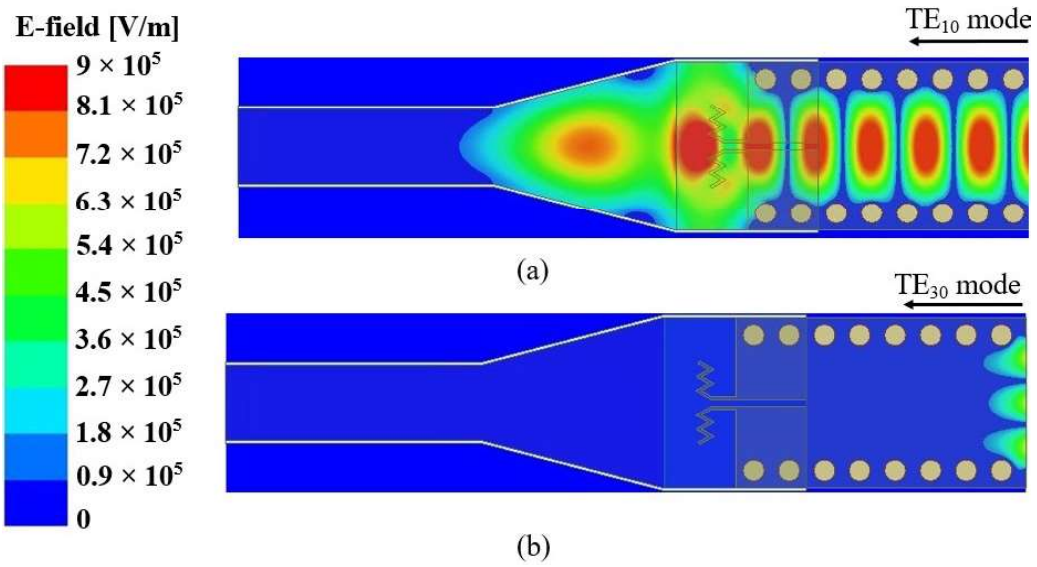

Figure 6. Simulated E-field distribution of the proposed converter at 2.25 THz when the SIW was applied in (**a**) TE_{10} and (**b**) TE_{30} mode.

4.3. Back-to-Back RWG TE_{10} to RWG TE_{10} Converter

As shown in Figure 7, a full back-to-back mode converter was designed. In this design, the guided TE_{10} mode of the RWG is converted into the TE_{20} mode of the SIW and then back to the RWG's TE_{10} mode.

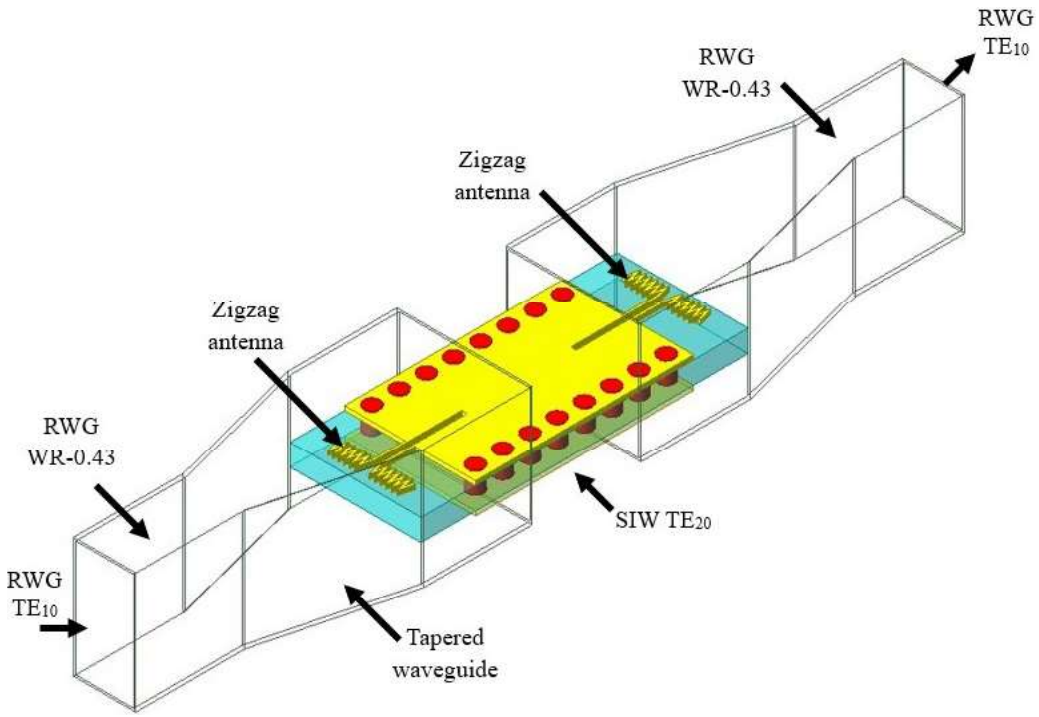

Figure 7. An isometric view of the proposed back-to-back TE_{10}–TE_{10} mode converter.

The simulated results of the proposed back-to-back mode converter are shown in Figure 8 with variation in four significant design parameters: l_1, l_2, α, and the number of zigzag antenna arms (N). This converter has a 380 µm length and uses a polyimide substrate with a dielectric constant of 3.5 and loss tangent (tan δ) of 0.008. Figure 8a,b shows the magnitude of the reflection coefficient $|S_{11}|$ for the TE_{10}–TE_{10} back-to-back mode converter at different values of l_1 and l_2. These values were adjusted to achieve the proper impedance matching across the converter's operating region, specifically the bandwidth and the center frequency. Likewise, the zigzag antenna in Figure 3b consists of two important features: the number of arms (N) and the angle between them (α). From Figure 8c,d, we can see that the number of arms affected the magnitude of the transmission coefficient $|S_{21}|$ for the TE_{10}-to-TE_{10} mode converter more than the angle between those arms. Therefore, the primary objective for minimizing the insertion loss in the mode converter was using fewer zigzag arms. After design and simulation followed by the optimization process, the complete dimensional parameter of the mode converter is shown in Table 1.

Table 1. Design parameters for the proposed mode converter.

Parameters	w_{rwg}	h_{rwg}	l_{twg}	l_{wwg}	h_{uwwg}	h_{dwrwg}
Values (µm)	53	106	130	100	57.5	29
Parameters	h_{sub}	p_{via}	d_{via}	w_{slot}	w_{siw}	w_{sub}
Values (µm)	20	25	14	5	95	120
Parameters	l_1	l_2	w_2	l_{zaizag}	α	w_{twg}
Values (µm)	17	53	2	10	55°	57

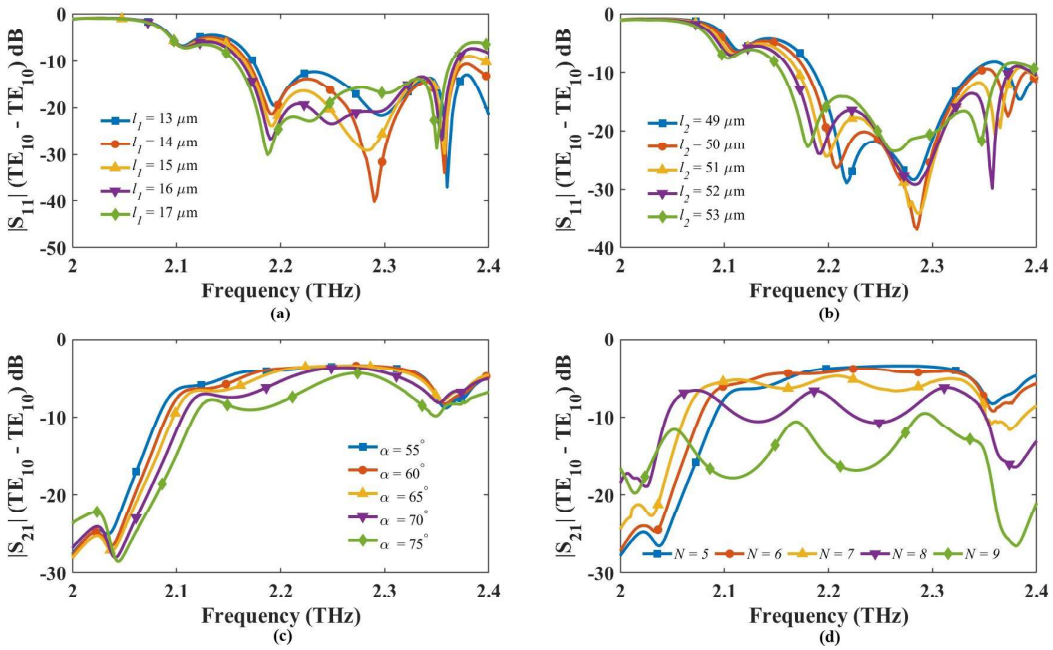

Figure 8. Simulated $|S_{11}|$ (TE_{10}-TE_{10}) of the back-to-back converter at different values for (**a**) l_2 and (**b**) l_3 and $|S_{21}|$ (TE_{10}-TE_{10}) at different values for (**c**) the angle between two arms of the zigzag antenna and (**d**) the number of arms in the zigzag antenna.

4.4. Equivalent Circuit Model and Design Guidelines for the Mode Converter

For the RWG in TE_{10} mode, the characteristic impedance is the product between the wave impedance and the short side to long side ratio of the RWG [34], given by

$$Z_{\mathrm{rwg}} = \frac{w_{\mathrm{rwg}}}{h_{\mathrm{rwg}}} Z_{rwg}^{\mathrm{TE10}} \tag{11}$$

where w_{rwg}, h_{rwg}, and $Z_{\mathrm{rwg}}^{\mathrm{TE10}}$ represent the width, height, and wave impedance of the RWG, respectively. Similarly, the characteristic impedance of the widened waveguide and the SIW are given as follows:

$$Z_{\mathrm{wwg}} = \frac{w_{\mathrm{wwg}}}{h_{\mathrm{rwg}}} Z_{\mathrm{rwg}}^{\mathrm{TE10}} \tag{12}$$

$$Z_{\mathrm{siw}} = \frac{h_{\mathrm{sub}}}{w_{\mathrm{eqv}}} Z_{\mathrm{siw}}^{\mathrm{TE10}} \tag{13}$$

where w_{wwg}, h_{wwg}, $Z_{\mathrm{twg}}^{\mathrm{TE10}}$, h_{sub}, w_{eqv}, and $Z_{\mathrm{siw}}^{\mathrm{TE10}}$ represent the width, height, and wave impedance of the widened waveguide and SIW, respectively. Detailed calculations for the wave impedance of the RWG and SIW can be found in [35]. In Equation (12), the characteristic impedance of the widened waveguide is higher than that of the RWG. This is because the transition waveguide (i.e., the tapered waveguide) provides a smooth conversion from the RWG to the widened waveguide by minimizing the reflection and impedance mismatch. It achieves this by gradually changing the wave impedance and E-field distribution between the RWG and the widened waveguide [36–38].

The equivalent circuit diagram of the proposed converter, featuring lumped elements, characteristic impedance, and coupling transformers, is shown in Figure 9. A similar equivalent circuit can be found in [39] for the microstrip-to-waveguide transition, [40] for the slot-line transition to the double-sided parallel-strip line of a magic-T, [10] for the transition from a slot-line to SIW and aperture coupling to SIW, and [9] for the RWG-to-SIW transition. In our design, T_1 represents the coupling coefficient between the RWG and aperture slot-line, while T_2 denotes the coupling between the slot-line and the SIW

operating in TE_{20} mode. During this mode conversion, the electric field is zero at the center of the symmetrical plane (x-y plane), effectively acting as a virtual ground. The E-field exhibited equal magnitudes but opposite directions on either side, as illustrated in Figure 4. This behavior, from a circuit perspective, resembles a differential pair with positive and negative terminals, making the slot-line and the TE_{20} mode SIW a differential port. The lumped elements are determined as follows. C_1 and L_1 represent the capacitive and inductive elements, respectively, based on the dimensions of the slot-line (w_{slot} and l_2) [10]. Similarly, C_2 and L_2 in the SIW account for energy storage due to capacitive discontinuity during mode conversion from a slot-line to the SIW's TE_{20} mode. They also represent magnetic energy storage caused by the metallic via array within the SIW [9].

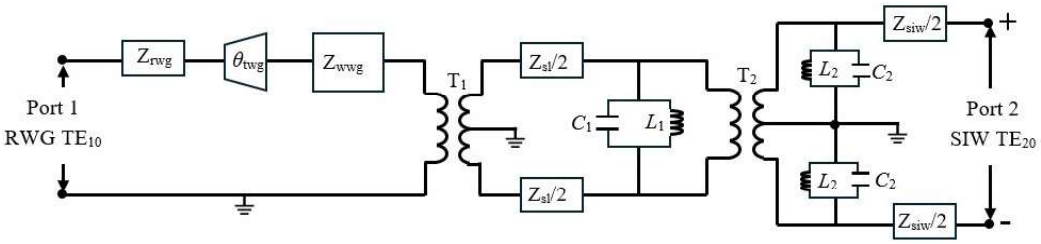

Figure 9. Equivalent circuit for the proposed RWG TE_{10} to SIW TE_{20} mode converter.

The primary operating principle of the proposed mode converter, converting from a TE_{10} mode RWG to a TE_{20} mode SIW, according to the circuit analysis, is based on impedance matching between the RWG and SIW as well as converting the unbalanced RWG port to a balanced differential SIW port. This process increases the complexity of the circuit design due to the difficulty in accurately estimating the relationship between the structure parameters and the values of electrical components. Thus, theoretical analysis combined with simulation software optimization is necessary to to achieve mode conversion. A flow chart algorithm, depicted in Figure 10, outlines the steps for achieving mode conversion.

The design goal was to achieve successful mode conversion from a TE_{10} mode RWG to a TE_{20} mode SIW. The geometrical parameters of the RWG were based on the standard WR-0.43 dimensions, as defined by the IEEE standards [41]. Detailed analysis and methods for calculating the length (electrical length θ_{twg}) of the tapered waveguide can be found in [38]. For the initial dimensions of the SIW, Section 3 provides the theoretical analysis and the formulas, which are dependent on the operating frequency range of the design. The dimensions of the zigzag antenna must be chosen to ensure resonance within the operational frequency range of the mode converter, enabling the maximum transfer of EM energy to the aperture slot. The aperture slot's length (l_2) should initially be set to half of the guided wavelength, while its width (w_{slot}) must be small enough to allow the E-field to pass through the symmetrical plane of the slot. Finally, the model was implemented in the Ansys high-frequency structure simulator (HFSS) computational software for analysis. To achieve the design goal of a return loss of less than 10 dB and proper impedance matching, the dimensional parameters were optimized using the built-in sequential, nonlinear optimization algorithm.

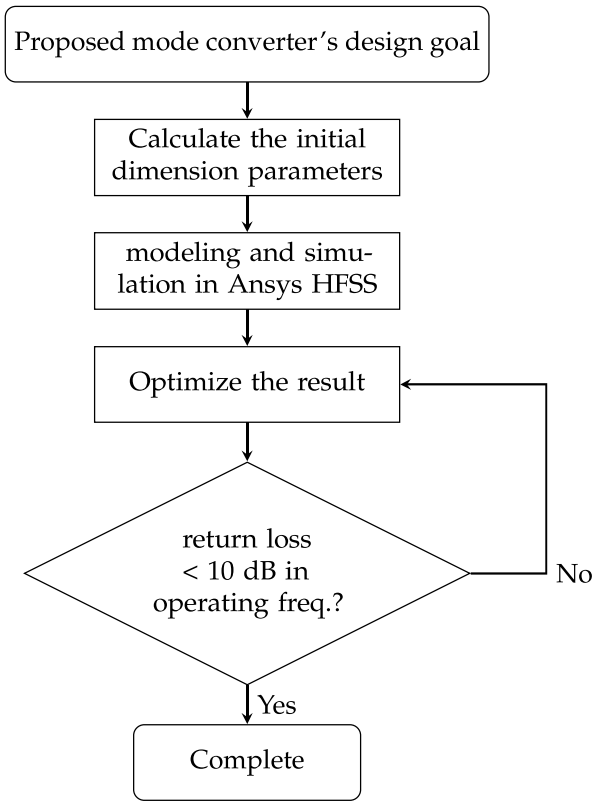

Figure 10. Flowchart for the design process of the proposed RWG TE_{10} to SIW TE_{20} mode converter.

5. THz On-Chip Antenna Based on SIW TE_{20} Mode

In this section, we propose an on-chip antenna (OCA) with an L-shaped radiating patch on the top metallic layer of the substrate integrated waveguide (SIW) to increase the radiating aperture and maximize the efficiency and gain [8,14,42], as shown in Figure 11a.

Various methods have been proposed to enhance OCA performance, such as adding a superstrate layer [43] or using artificial magnetic conductors (AMCs) [44]. However, challenges like backside lobes and surface waves persist. To address these issues, we fed the OCA with the TE_{20} mode of the SIW. Compared with the TE_{10} mode, the TE_{20} mode features a higher-order electric field distribution, resulting in a more uniformly distributed field across the radiating patch, which improves the gain and bandwidth [45]. Additionally, since the cutoff frequency of the TE_{20} mode is higher than that of the TE_{10} mode, this higher mode enables the higher operating frequencies and increases the channel capacity [46].

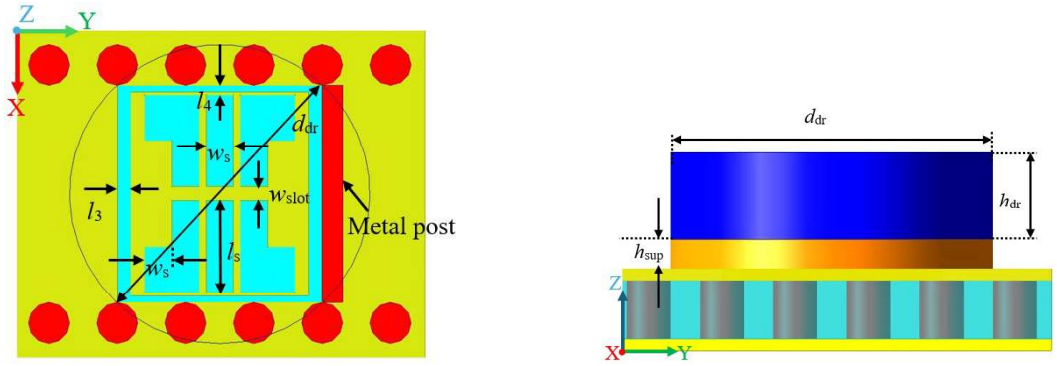

(a) (b)

Figure 11. Antenna geometry: (**a**) top view and (**b**) side view.

We added a dielectric resonator (DR) and supporting layers to improve impedance matching between the DR and the radiating patch, further increase the bandwidth, and

find the desired polarization characteristics [13,14]. To maximize the antenna performance, the dielectric layer's dimensions and properties were changed [47].

A common issue with OCA performance is radiation leakage into the surrounding circuit, which is addressed in this model by introducing a metallic wall adjacent to the radiating patch [14,19]. This design forms an OCA with a yagi-like structure, where the DR acts as the director and the radiating slot serves as the driver, with the reflector omitted [13]. We evaluated the OCA performance using a cylinder-shaped DR placed on top of the radiating slots. Both the DR and supporter structures shared the same diameter d_{dr}. The DR was made of silicon, with a dielectric constant (ϵ_{dr}) of 11.9, while the supporting structure was made of Roger RT/duroid 5880, which has a dielectric constant of (ϵ_{sup}) of 2.2.

The simulated results of the proposed DR-based OCA fed by the TE_{20} mode of the SIW are shown in Figure 12. The thickness of the DR was directly proportional to the guided wavelength λ_{dr} and inversely proportional to the dielectric constant (ϵ_{dr}) of the DR [48]. We examined the $|S_{11}|$ and the gain of the antenna by adjusting the thickness of the DR and its supporting structure. The $|S_{11}|$ and gain parameters were significantly influenced by the thickness of the DR. In contrast, variations in the support structure thickness resulted in minimal changes in the magnitude reflection coefficient and gain. Thus, in the case of a DR-based OCA, the DR thickness plays a crucial role in maximizing the gain and achieving a larger bandwidth. The optimized parameters for the slots and DR were as follows: l_3 = 5, l_4 = 2.5, w_s = 10, l_s = 34, h_{dr} = 25, h_{sup} = 5, and d_{dr} = 110 (all dimensions are in μm). With these dimensions, the antenna achieved a maximum gain of 4.49 dB at a frequency of 2.32 THz. The distribution of the E-field and the corresponding 3D radiation pattern are shown in Figure 13. Even though the TE_{20} mode SIW had two lobes with a space in between them, the radiation pattern of the patch antenna typically radiated a broadside pattern, giving a single main lobe and sometimes additional side lobes, depending upon the shape and size of the patch, which we could see for other higher-mode SIW patch antennas [14,15,49].

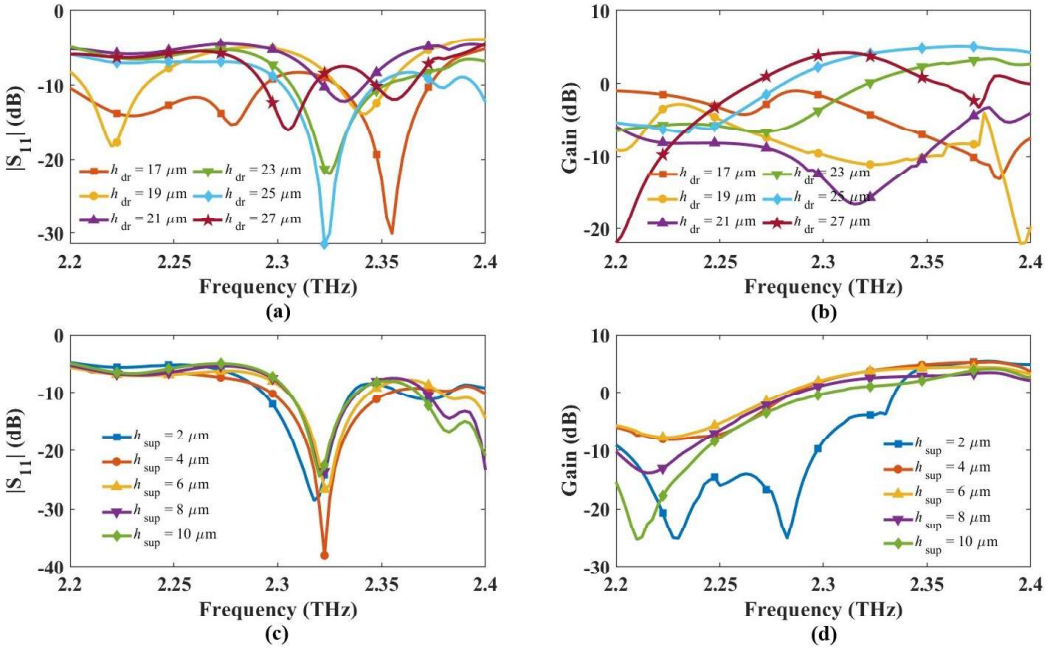

Figure 12. Simulated results of antenna performance: (**a**) reflection coefficient $|S_{11}|$ and (**b**) gain at different thickness of the dielectric substrate (h_{dr}); (**c**) reflection coefficient $|S_{11}|$ and (**d**) gain at different thickness of the supporter (h_{sup}).

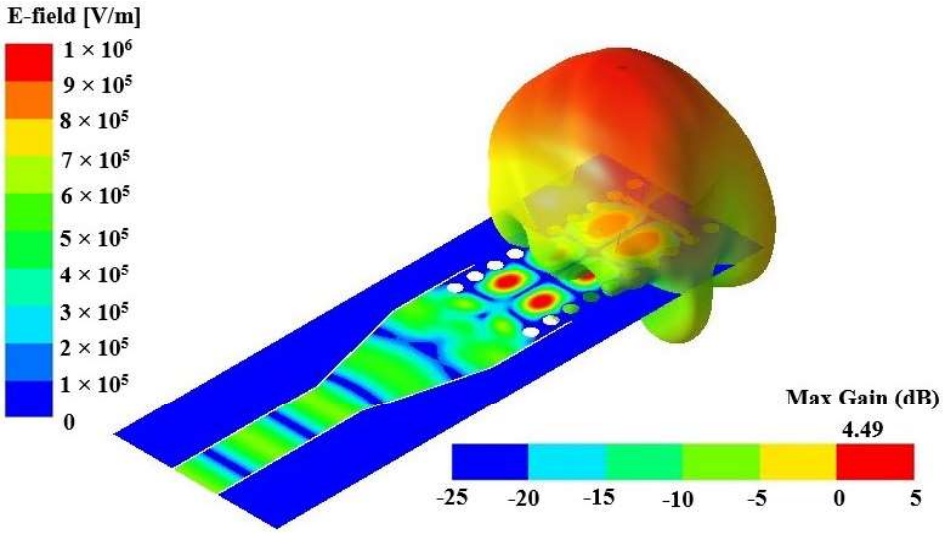

Figure 13. Isometric view of E-field of TE_{20} mode SIW overlay with 3D radiation plot.

6. THz SIW Balun Based on TE_{20} Mode

A balun (from balanced to unbalanced) is an RF circuit that achieves the balanced signal from the unbalanced and vice versa. It is a power splitter that has two outputs with equal magnitudes but 180° out of phase with each other. An unbalanced port carries the signal in one conductor and is grounded in another conductor, whereas a balanced or differential port uses both conductors to carry the signal which is 180° out of phase with the other one.

Since a balun is a reciprocal device (i.e., the transmission characteristic is the same in both directions), it can be expressed in terms of the *S*-parameters as follows:

$$S_{31} = S_{13} = -S_{21} = -S_{12} \tag{14}$$

A balun allows the balanced and unbalanced line circuits to be interfaced. The TE_{20} mode SIW had equal and opposite phases on both sides of the symmetric plane, which was analogous to the electric field distribution between the two ports of the balun. A balun based on the TE_{20} mode SIW could be achieved because the electric field distribution in the TE_{20} mode SIW had an equal magnitude but opposite direction in the symmetrical plane (X–Y), which is analogous to the balanced port of a balun. A balun designed based on the proposed mode converter is depicted in Figure 14.

In this balun, the two half-modes of the TE_{20} mode SIW were split into two ports (port 2 and port 3) symmetrically in the x plane at an angle of 45°, being guided by the metallic vias successfully, and the electric field at 2.25 THz is shown in Figure 15. For both port 2 and port 3, the E-field distribution was for the TE_{10} mode SIW, which can be changed into the quasi-TEM mode of the microstrip line by using a tapered line in the absence of vias [9]. This is crucial for RF circuit elements, such as in a dipole antenna (balanced ports 2 and 3) for the requirement of an unbalanced signal (port 1) from a coaxial cable [50]. Furthermore, in the case of the antenna array, this ensures that the signal is divided and fed appropriately to the respective elements [51].

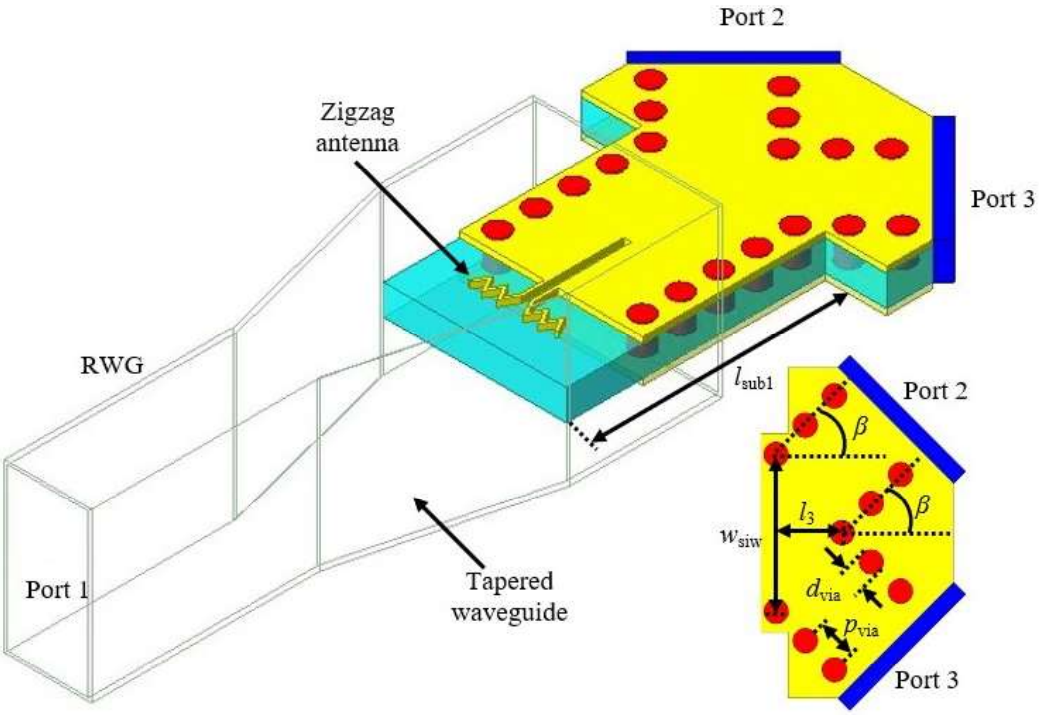

Figure 14. Isometric view of the proposed balun based on the TE_{20} mode of an SIW. The major dimensions are l_3 = 41.25 µm and $\beta = 45^{\circ}$, with the rest provided in Table 1.

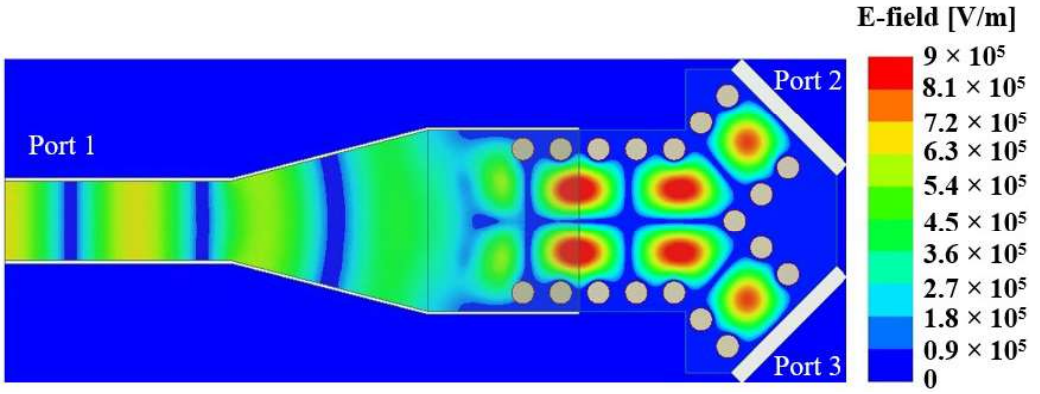

Figure 15. Simulated E-field distribution of THz SIW balun based on TE_{20} mode.

Figure 16 shows the simulated results of the balun. It is shown that the proposed balun's $|S_{11}|$ parameter was better than −10 dB in the frequency range of 2.15–2.35 THz, with an intrinsic insertion loss of about 5.3–6.5 dB. Likewise, the amplitude imbalance for the differential ports (port 2 and port 3) was ± 0.037 dB, and the phase imbalance was less than 1° over the operating frequency range of the balun.

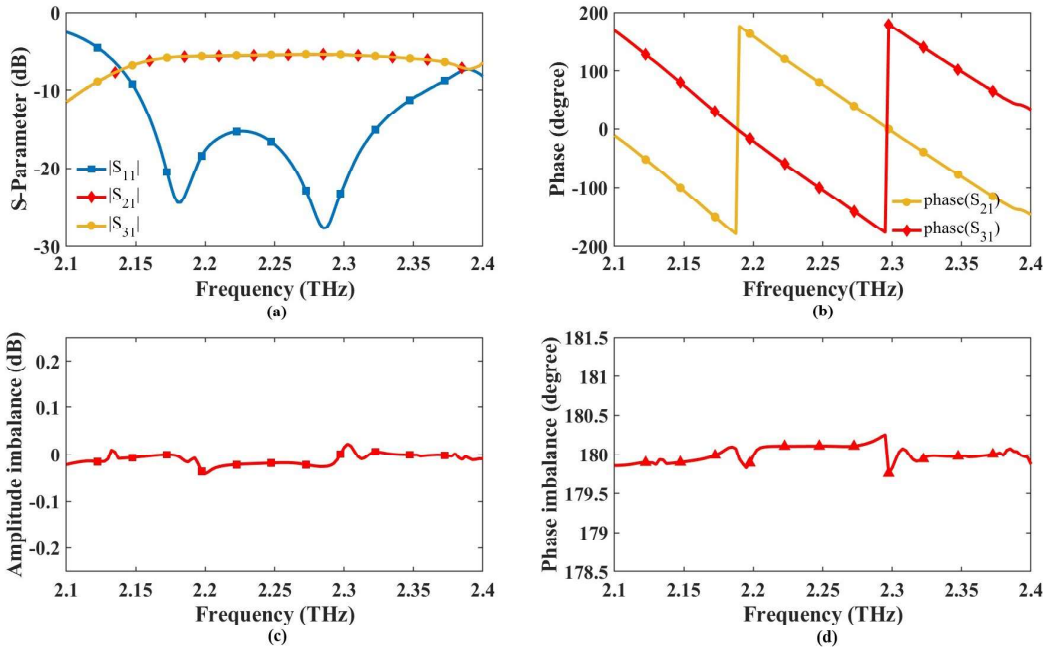

Figure 16. Simulated results of THz SIW balun based on TE_{20} mode. (**a**) *S*-parameter, (**b**) phase of port 2 and 3, (**c**) amplitude imbalance between balanced ports, and (**d**) phase imbalance between balanced ports.

A detailed comparison of the proposed mode converter with existing converters in the literature is provided in Table 2, which provides the details of the mode conversion architecture. Most of the available mode converters operate at lower frequencies, ranging from microwave to millimeter wave bands, with limited research conducted at higher frequencies (THz range or above 300 GHz). By combining a zigzag antenna and an aperture coupling slot, this paper effectively demonstrates the conversion of a TE_{10} mode RWG to a TE_{20} mode SIW for planar integration.

Table 2. Comparison of the proposed mode converter with the available converter from the literature.

Reference	Frequency (GHz)	Method	Type	Mode	Layers	$\|S_{11}\|$ dB	$\|S_{21}\|$ dB
[9]	198–238	Dipole antenna slotline	RWG to SIW	TE_{10} to TE_{20}	single	<−6	1.1–2.5
[10]	7.3–11.6 8.34–12.58	Slotline aperture and MS-line	Slotline to SIW MS-line to SIW	TEM to TE_{20}	single double	<−10	1.5–2.6 2.1
[12]	23.83–40	Stepped RWG and multi-section SIW	RWG to SIW	TE_{10} to TE_{10}	single	<−15	<2.45
[4]	32–50	Height-stepped RWG	RWG to SIW	TE_{10} to TE_{10}	single	<−15	0.68
[19]	180–240	Stepped dielectric coupling aperture	RWG to SIW	TE_{10} to TE_{10}	double	<−10	<0.9
[11]	228–293	T-junction power divider	RWG to RWG	TE_{10} to TE_{20}	single	<−15	<1
[52]	28–38	Right-angled waveguide coupling	RWG to RWG	TE_{01} to TE_{20}	single	<−19	3
[23]	11.28–14.8	Power divider and phase shifter	RWG to RWG	TE_{10} to TE_{30}	single	<−10	3
This work	2.15–2.36 THz	Zigzag antenna aperture slot	RWG to SIW	TE_{10} to TE_{20}	single	<−10	5

7. Conclusions

In this paper, we propose a RWG TE_{10} to SIW TE_{20} mode converter using a tapered waveguide, widened waveguide, zigzag antenna, and coupling slot in the THz band. A back-to-back mode converter from RWG TE_{10} to RWG TE_{10} was also developed, achieving an average intrinsic insertion loss of 5 dB and a return loss better than −10 dB over the frequency range of 2.15–2.36 THz. An equivalent circuit of the proposed converter was provided along with the design process to achieve efficient conversion. Leveraging the advantages of a higher-order mode, an on-chip antenna with a dielectric resonator was designed to be fed by the TE_{20} mode of a SIW, achieving a maximum gain of 4.49 dB. Furthermore, based on the RWG-to-SIW transition, a balun was designed, resulting in a phase imbalance of less than 1° between different ports, verifying the existence of the TE_{20} mode with an equal magnitude but opposite phase. The proposed mode converter is a planer, making it suitable for future THz integrated circuits, along with its wide band performance and the ability to transition to a single higher-order mode.

Author Contributions: Conceptualization, B.P.; Methodology, B.P.; Validation, X.J.L.; Formal analysis, X.J.L.; Investigation, B.P.; Writing—original draft, B.P.; Writing—review & editing, X.J.L. and B.-C.S.; Supervision, X.J.L. and B.-C.S. All authors have read and agreed to the published version of the manuscript.

Funding: This research received no external funding.

Data Availability Statement: All the data are available within the manuscript.

Conflicts of Interest: The authors declare no conflicts of interest.

References

1. Paudel, B.; Li, X.J.; Seet, B.C. Design and Modeling of a Terahertz Transceiver for Intra-and Inter-Chip Communications in Wireless Network-on-Chip Architectures. *Sensors* **2024**, *24*, 3220.
2. Jiang, W.; Zhou, Q.; He, J.; Habibi, M.A.; Melnyk, S.; El-Absi, M.; Han, B.; Di Renzo, M.; Schotten, H.D.; Luo, F.L.; et al. Terahertz communications and sensing for 6G and beyond: A comprehensive review. *IEEE Commun. Surv. Tutorials* **2024**, *26*, 2326–2381.
3. Chakraborty, D.; Boni, R.; Mills, B.N.; Cheng, J.; Komissarov, I.; Gerber, S.A.; Sobolewski, R. High-Density Polyethylene Custom Focusing Lenses for High-Resolution Transient Terahertz Biomedical Imaging Sensors. *Sensors* **2024**, *24*, 2066.
4. Cano, J.; Mediavilla, A.; Perez, A. Full-Band Air-Filled Waveguide-to-Substrate Integrated Waveguide (SIW) Direct Transition. *IEEE Microw. Wirel. Components Lett.* **2015**, *25*, 79–81. https://doi.org/10.1109/LMWC.2014.2372480.
5. Wu, K.; Deslandes, D.; Cassivi, Y. The substrate integrated circuits-a new concept for high-frequency electronics and optoelectronics. In Proceedings of the 6th International Conference on Telecommunications in Modern Satellite, Cable and Broadcasting Service, TELSIKS, Nis, Serbia, 1–3 October 2003; IEEE: Piscataway, NJ, USA 2003; Volume 1, pp. P–III.
6. Sun, L.; Zhang, Y.; Cai, Y.; Qian, Z. Wideband excitation technology of substrate integrated waveguide TE_{30} mode and its antenna application. *Electron. Lett.* **2017**, *53*, 828–830.
7. Paudel, B.; Li, X.J.; Seet, B.C. Using Terahertz On-Chip Antennas for Intra-Chip Wireless Communications within a Multi-core Processor. In Proceedings of the 2024 49th International Conference on Infrared, Millimeter, and Terahertz Waves (IRMMW-THz), Espoo, Finland, 1–6 September 2024; IEEE: Piscataway, NJ, USA, 2024; pp. 1–2.
8. Paudel, B.; Li, X.J. A Terahertz On-Chip Antenna for Intra-chip Wireless Communications. In Proceedings of the 2022 IEEE Conference on Antenna Measurements and Applications (CAMA), Guangzhou, China, 14–17 December 2022; pp. 1–3. https://doi.org/10.1109/CAMA56352.2022.10002470.
9. Yu, B.; Wang, Z.; Zhu, H.; Yan, B.; Xu, R.; Xu, Y. A Broadband 220-GHz Converter From Rectangular Waveguide TE_{10} Mode to SIW TE_{20} Mode for Terahertz Planar Integration. *IEEE Trans. Microw. Theory Tech.* **2024**, *72*, 6956–6967. https://doi.org/10.1109/TMTT.2024.3412744.
10. Wu, P.; Liu, J.; Xue, Q. Wideband Excitation Technology of TE_{20} Mode Substrate Integrated Waveguide (SIW) and Its Applications. *IEEE Trans. Microw. Theory Tech.* **2015**, *63*, 1863–1874.
11. Shu, G.; Qian, Z.; He, W. Design and measurement of an H-band rectangular TE 10 to TE 20 mode converter. *IEEE Access* **2020**, *8*, 37242–37249.
12. Li, T.; Meng, H.; Dou, W. Broadband transition between substrate integrated waveguide and rectangular waveguide based on ridged steps. *IEICE Electron. Express* **2014**, *11*, 20140434–20140434.

13. Deng, X.D.; Li, Y.; Liu, C.; Wu, W.; Xiong, Y.Z. 340 GHz on-chip 3-D antenna with 10 dBi gain and 80% radiation efficiency. *IEEE Trans. Terahertz Sci. Technol.* **2015**, *5*, 619–627.
14. Wu, P.; Liu, K.; Yu, Z. 220 GHz high-gain substrate integrated antennas with low fabrication cost based on higher order mode and PCB technology. *IEEE Trans. Antennas Propag.* **2022**, *71*, 18–28.
15. Wu, P.; Liao, S.; Xue, Q. Wideband excitations of higher-order mode substrate integrated waveguides and their applications to antenna array design. *IEEE Trans. Antennas Propag.* **2017**, *65*, 4038–4047.
16. Dong, J.; Liu, Y.; Yang, Z.; Peng, H.; Yang, T. Broadband millimeter-wave power combiner using compact SIW to waveguide transition. *IEEE Microw. Wirel. Components Lett.* **2015**, *25*, 567–569.
17. Wong, S.W.; Wang, K.; Chen, Z.N.; Chu, Q.X. Design of millimeter-wave bandpass filter using electric coupling of substrate integrated waveguide (SIW). *IEEE Microw. Wirel. Components Lett.* **2013**, *24*, 26–28.
18. Abdel-Wahab, W.M.; Safavi-Naeini, S. H-plane metallic RWG-to-SIW transition using aperture coupling. In Proceedings of the 2019 IEEE International Symposium on Antennas and Propagation and USNC-URSI Radio Science Meeting, Atlanta, GA, USA, 7–12 July 2019; IEEE: Piscataway, NJ, USA, 2019; pp. 963–964.
19. Liu, K.; Wu, P.; Zhang, J. Wideband RWG-SIW interconnection with improved integration for millimeter-wave/terahertz application. *IEEE Microw. Wirel. Components Lett.* **2022**, *32*, 835–838.
20. Li, Y.; Luk, K.M. A broadband V-band rectangular waveguide to substrate integrated waveguide transition. *IEEE Microw. Wirel. Components Lett.* **2014**, *24*, 590–592.
21. Li, T.; Dou, W.; Meng, H. Wideband transition between substrate integrated waveguide (SIW) and rectangular waveguide (RWG) based on bend waveguide. In Proceedings of the 2014 Asia-Pacific Microwave Conference, Sendai, Japan, 4–7 November 2014; IEEE: Piscataway, NJ, USA, 2014; pp. 438–440.
22. Sarkar, A.; Sharma, A.; Biswas, A.; Akhtar, M.J. Compact CRLH leaky-wave antenna using TE 20-mode substrate-integrated waveguide for broad space radiation coverage. *IEEE Trans. Antennas Propag.* **2020**, *68*, 7202–7207.
23. Zhang, Y.; Wang, G.; Hong, W. Design and verification of broadband substrate integrated waveguide TE_{10}-TE_{30} mode converter. *IEEE Trans. Microw. Theory Tech.* **2023**, *72*, 1176–1186.
24. Wang, G.; Zang, H.; Dong, Z.; Zhu, X.; Zhang, Y. Systematic Design of Substrate Integrated Waveguide TE 10-TE N0-Mode Converter. In Proceedings of the 2023 IEEE MTT-S International Microwave Workshop Series on Advanced Materials and Processes for RF and THz Applications (IMWS-AMP), Chengdu, China, 13–15 November 2023; IEEE: Piscataway, NJ, USA, 2023; pp. 1–3.
25. Passi, D.; Leggieri, A.; Citroni, R.; Di Paolo, F. Broadband TE10 to TE20 mode transformer for X band. *Adv. Electromagn.* **2016**, *5*, 69–72.
26. Bozzi, M.; Pasian, M.; Perregrini, L. Modeling of losses in substrate integrated waveguide components. In Proceedings of the 2014 International Conference on Numerical Electromagnetic Modeling and Optimization for RF, Microwave, and Terahertz Applications (NEMO), Pavia, Italy, 14–16 May 2014; IEEE: Piscataway, NJ, USA, 2014; pp. 1–4.
27. Kordiboroujeni, Z.; Bornemann, J. Designing the width of substrate integrated waveguide structures. *IEEE Microw. Wirel. Components Lett.* **2013**, *23*, 518–520.
28. Jia, M.; Zhang, J.; Dong, Y. A compact and broadband balun based on multilayer SIW. *IEEE Microw. Wirel. Components Lett.* **2021**, *32*, 105–108.
29. Pozar, D.M. *Microwave Engineering: Theory and Techniques*; John Wiley & Sons: Hoboken, NJ, USA, 2021.
30. Lee, S.; Mei, K. Analysis of zigzag antennas. *IEEE Trans. Antennas Propag.* **1970**, *18*, 760–764.
31. Narde, R.S.; Venkataraman, J.; Ganguly, A.; Puchades, I. Intra-and inter-chip transmission of millimeter-wave interconnects in NoC-based multi-chip systems. *IEEE Access* **2019**, *7*, 112200–112215.
32. Lindell, I.V.; Sihvola, A. *Boundary Conditions in Electromagnetics*; John Wiley & Sons: Hoboken, NJ, USA, 2019.
33. Zehentner, J.; Machac, J.; Mrkvica, J. Even and odd modes on a conductor-backed slotline. In Proceedings of the 2002 32nd European Microwave Conference, Milan, Italy, 23–26 September 2002; IEEE: Piscataway, NJ, USA, 2002; pp. 1–4.
34. Herhil, Y.; Piltyay, S.; Bulashenko, A.; Bulashenko, O. Characteristic impedances of rectangular and circular waveguides for fundamental modes. In Proceedings of the 2021 IEEE 3rd Ukraine Conference on Electrical and Computer Engineering (UKRCON), Lviv, Ukraine, 26–28 August 2021; IEEE: Piscataway, NJ, USA, 2021; pp. 46–51.
35. Jin, J.M. *Theory and Computation of Electromagnetic Fields*; John Wiley & Sons: Hoboken, NJ, USA, 2015.
36. Sangam, R.S.; Kshetrimayum, R.S. Linear tapers: analysis, design and applications. In Proceedings of the 2018 IEEE MTT-S International Microwave and RF Conference (IMaRC), Kolkata, India, 28–30 November 2018; IEEE: Piscataway, NJ, USA, 2018; pp. 1–4.
37. Deslandes, D. Design equations for tapered microstrip-to-substrate integrated waveguide transitions. In Proceedings of the 2010 IEEE MTT-S International Microwave Symposium, Anaheim, CA, USA, 23–28 May 2010; IEEE: Piscataway, NJ, USA, 2010; pp. 704–707.

38. Alam, A.; Alam, M.S.; AlMuhanna, K.; Zhang, H.; Shamim, A.; Shamsan, Z.A. A wideband transition design technique from RWG to SIW technologies. *IEEE Access* **2023**, *11*, 109539–109552.
39. Huang, X.; Wu, K.L. A broadband U-slot coupled microstrip-to-waveguide transition. *IEEE Trans. Microw. Theory Tech.* **2012**, *60*, 1210–1217.
40. Feng, W.; Xue, Q.; Che, W. Compact planar magic-T based on the double-sided parallel-strip line and the slotline coupling. *IEEE Trans. Microw. Theory Tech.* **2010**, *58*, 2915–2923.
41. IEEE Standard for Rectangular Metallic Waveguides and Their Interfaces for Frequencies of 110 GHz and Above—Part 1: Frequency Bands and Waveguide Dimensions. *IEEE STD* **2013**, *2013*, 1–22. https://doi.org/10.1109/IEEESTD.2013.6471987.
42. Paudel, B.; Li, X.J.; Seet, B.C. A 254–276 GHz On-Chip THz Antenna Using Substrate Integrated Waveguide and Metamaterials for Short-Range Wireless Communications. In Proceedings of the 2023 IEEE Region 10 Symposium (TENSYMP), Canberra, Australia, 6–8 September 2023; pp. 1–6. https://doi.org/10.1109/TENSYMP55890.2023.10223667.
43. Khan, M.A.K.; Ullah, M.I.; Kabir, R.; Alim, M.A. High-performance graphene patch antenna with superstrate cover for terahertz band application. *Plasmonics* **2020**, *15*, 1719–1727.
44. Althuwayb, A.A.; Alibakhshikenari, M.; Virdee, B.S.; Benetatos, H.; Falcone, F.; Limiti, E. Antenna on chip (AoC) design using metasurface and SIW technologies for THz wireless applications. *Electronics* **2021**, *10*, 1120.
45. Jin, H.; Che, W.; Chin, K.S.; Yang, W.; Xue, Q. Millimeter-wave TE 20-mode SIW dual-slot-fed patch antenna array with a compact differential feeding network. *IEEE Trans. Antennas Propag.* **2017**, *66*, 456–461.
46. Suntives, A.; Abhari, R. Design and application of multimode substrate integrated waveguides in parallel multichannel signaling systems. *IEEE Trans. Microw. Theory Tech.* **2009**, *57*, 1563–1571.
47. Keyrouz, S.; Caratelli, D. Dielectric resonator antennas: Basic concepts, design guidelines, and recent developments at millimeter-wave frequencies. *Int. J. Antennas Propag.* **2016**, *2016*, 6075680.
48. Petosa, A. *Dielectric Resonator Antenna Handbook*; Artech: Morristown, NJ, USA, 2007.
49. Wu, P.; Chen, Y.; Ren, Y.; Yu, Z. Terahertz Antenna on Chip (AoC) Solutions with Improved Structure Using Higher-Order Modes. In Proceedings of the 2024 49th International Conference on Infrared, Millimeter, and Terahertz Waves (IRMMW-THz), Perth, Australia, 1–6 September 2024; IEEE: Piscataway, NJ, USA, 2024; pp. 1–4.
50. Cai, Z.; Weng, Z.; Qi, Y.; Fan, J.; Zhuang, W. A high-performance standard dipole antenna suitable for antenna calibration. *IEEE Trans. Antennas Propag.* **2021**, *69*, 8878–8883.
51. Lou, J.; Jin, X.; Wang, J.; Zhou, Y.; Liu, S. 0.9 to 11.9 GHz Ultrabroadband Phased Array Antenna Feeding by Double-Y Balun. In Proceedings of the 2024 International Conference on Microwave and Millimeter Wave Technology (ICMMT), Qingdao, China, 14–17 May 2024; IEEE: Piscataway, NJ, USA, 2024; Volume 1, pp. 1–3.
52. Zhao, P.; Wang, Q.; Deng, J. A novel broadband rectangular waveguide TE 01–TE 20 mode converter. *IEEE Microw. Wirel. Components Lett.* **2018**, *28*, 747–749.